Dalton Transactions

PAPER

View Article Online
View Journal

Cite this: DOI: 10.1039/d6dt00780e

Hydrogen bond enhanced coordination of hydrogen peroxide to indium trichloride

Nikita S. Mayorov, [a] Pavel A. Egorov, [a] Alexander G. Medvedev, [a] Evgeny S. Belyaev, [b] Oleg A. Filippov, [c] Natalia V. Belkova, *[c] Alexey A. Mikhaylov, [a] Maxim N. Sokolov, [d] Ovadia Lev *[e] and Petr V. Prikhodchenko *[a]

Coordination of hydrogen peroxide by a metal center is the first step in the enzymatic cycle of peroxidases and catalases. Although this process occurs readily in living cells, synthesizing molecular complexes with the H_2O_2 ligand remains challenging due to hydrogen peroxide's weaker coordinating ability compared to other polar solvents. To date, structural information on coordination compounds with hydrogen peroxide as a ligand is represented by the crystal structures of a zinc complex and two tin complexes. This work demonstrates that hydrogen peroxide complexes can be prepared from coordinatively saturated compounds, such as indium(III) chloride. Ether compounds like 18-crown-6 or diethyl ether dissolve $InCl_3$, enabling its interaction with H_2O_2. Three $InCl_3$ complexes with hydrogen peroxide ligand, $[InCl_3(H_2O)_2(H_2O_2)]\cdot$18-crown-6, $[InCl_2(18\text{-crown-6})][(H_2O_2)InCl_4]$ and $[fac\text{-}InCl_3(H_2O_2)_{0.5}(H_2O)_{0.5}(18\text{-crown-6})]$, were isolated under different conditions, presenting a valuable addition to a very small family of structurally characterized H_2O_2 complexes. The crystal structures of these complexes were characterized by single-crystal X-ray diffraction analysis. DFT calculations unveiled the key role of the hydrogen bonding of the H_2O_2 ligand with ether molecules enhancing hydrogen peroxide coordination to In(III) center. Variable-temperature ^{1}H NMR data support the κ^1-coordination of H_2O_2 with $InCl_3$ in ethereal solution.

Received 5th April 2026,
Accepted 4th June 2026

DOI: 10.1039/d6dt00780e

rsc.li/dalton

Introduction

Hydrogen peroxide is a vital natural metabolite produced during cellular respiration.[1,2] The primary mechanism for regulating intracellular hydrogen peroxide concentration involves enzymatic reduction. In this process, hydrogen peroxide coordinates with the enzyme's active site to form a H_2O_2 molecular complex known as compound 0.[3,4] Similar to these biochemical processes, peroxidase-catalyzed hydrogen peroxide reduction finds widespread application in analytical chemistry[5,6] and various technologies.[7–10] Recent developments have focused on creating nanozymes with peroxidase-like activity for selective catalytic oxidation processes involving hydrogen peroxide.[11–13] Coordination with aluminum(III),[14] gallium(III), and indium(III)[15] has been proposed as a stage of hydrogen peroxide activation for the oxidation of hydrocarbons. Although hydrogen peroxide coordination to metal ions is often assumed to be straightforward in biochemical activation pathways, the isolation and characterization of true H_2O_2 complexes (as opposed to OOH^- or O_2^{2-} complexes) remains a significant challenge in synthetic chemistry. Williams *et al.* observed hydrogen peroxide's relatively weak affinity for Co(III) compared to aqua and OOH^- ligands, attributing this to the low basicity of H_2O_2.[16] The proton affinity of hydrogen peroxide is indeed 4.2 kcal mol^{-1} lower than that of water.[17] Mayer demonstrated that hydrogen peroxide cannot displace even the weakly bound perchlorate ligand in gallium porphyrinate complexes, suggesting that poor coordination ability is a general characteristic of peroxide chemistry unless deprotonation occurs.[18] This was further supported by ^{19}F, ^{45}Sc, ^{71}Ga, ^{115}In NMR studies that failed to detect hydrogen peroxide coordination to scandium(III), gallium(III), or indium(III) in 95–97 wt% H_2O_2 solutions of $K_3[ScF_6]$, $K_3[GaF_6]$, and $K_3[InF_6]$.[19]

Until recently, the absence of isolated, structurally characterized hydrogen peroxide complexes prevented explanation of their formation in aqueous solutions at the ultralow concen-

[a]N.S. Kurnakov Institute of General and Inorganic Chemistry, Russian Academy of Sciences, Leninskii pr. 31, Moscow 119991, Russian Federation. E-mail: prikhman@gmail.com
[b]Frumkin Institute of Physical Chemistry and Electrochemistry of the Russian Academy of Sciences, Leninskii pr. 31-4, Moscow 119071, Russian Federation
[c]A.N. Nesmeyanov Institute of Organoelement Compounds, Russian Academy of Sciences, Vavilov Str. 28, Moscow 119334, Russian Federation. E-mail: nataliabelk@ineos.ac.ru
[d]Nikolaev Institute of Inorganic Chemistry, Siberian Branch of the Russian Academy of Sciences, prosp. Academika Lavrentieva 3, 630090 Novosibirsk, Russian Federation
[e]Casali Center of Applied Chemistry, Hebrew University of Jerusalem, Jerusalem 9190401, Israel. E-mail: ovadia@mail.huji.ac.il

trations found in biological systems. The first crystal structure of a zinc–hydrogen peroxide complex revealed two hydrogen bonds between coordinated H_2O_2 and tosyl groups of adjacent ligands, suggesting the second coordination sphere plays a crucial role in the stabilization of hydrogen peroxide complex.[20] Subsequent NMR studies confirmed hydrogen peroxide coordination in analogous Co(III) complexes in non-aqueous solutions.[21] Recently, a new synthetic approach using coordinatively unsaturated p-block elements and neat hydrogen peroxide has been developed.[22] These H_2O_2 complexes were obtained in tin tetrachloride solutions (verified by NMR spectroscopy) and crystallized using 18-crown-6 as a second-sphere stabilizer. X-ray studies combined with DFT calculations demonstrated how primary and secondary interactions synergistically stabilize hydrogen peroxide ligands. In the present work, we successfully extended this approach to coordinatively saturated indium(III) chloride – a Lewis acid isoelectronic with tin(IV) chloride – chosen because In(III) better mimics peroxidase's Fe(III) center in size, charge, and polarizing ability.[23] Being formally tricoordinated, this compound is coordinatively saturated in the solid state that affects its solubility. A kaleidoscope of crystallized adducts provides new insights into $InCl_3$ dissolution and hydrogen peroxide coordination. NMR studies in diethyl ether solution support H_2O_2 coordination to indium despite the presence of competitive $Cl_3In\cdots OEt_2$ interactions. X-ray and DFT results highlight the importance of secondary H_2O_2 interactions, leading to a new concept of hydrogen bond-activated hydrogen peroxide coordination.

Results and discussion

Crystallization from $InCl_3$–H_2O_2–crown ether system

Indium(III) chloride is a solid under ambient conditions, with a layered structure formed by a roughly cubic close-packed arrangement of chloride ions and indium cations occupying octahedral voids between alternate pairs of anionic layers. The indium(III) coordination octahedra are linked into sheets parallel to the (001) plane.[24] $InCl_3$ dissolves readily in water but not in neat hydrogen peroxide. When placed in 99.9 wt% H_2O_2, $InCl_3$ crystals remained unchanged at the bottom of the vial, with only occasional gas bubbles released from their surface. Thus, we employed macrocyclic crown ethers not only as second-sphere stabilizers for the putative peroxide complex (a strategy successful for $SnCl_4$ complexes[22]) but also as ligands to solubilize coordinatively saturated $InCl_3$ in non-coordinating H_2O_2, given known precedents for crown ether–indium halide complexes.[25–27] To achieve this, liquid 15-crown-5 or a solution of 18-crown-6 in hydrogen peroxide was added to a dispersion of $InCl_3$ in H_2O_2, resulting in partial dissolution. The mixtures were kept overnight at −20 °C for crystallization. The resulting prismatic crystals were coated in perfluorinated oil and subjected to scXRD analysis. In addition, the obtained polycrystalline sample was analyzed by powder X-ray diffraction, recorded on a single-crystal diffractometer.

Surprisingly, scXRD revealed that the use of 15-crown-5 yields a disproportionation product: $[InCl_2(15\text{-crown-5})][InCl_4]$ (**1**; Fig. 1 and Fig. S1). The obtained diffraction pattern corresponds to the pattern simulated based on scXRD data for complex **1** (Fig. S2). Such ionic complexes are known for Group 13 M(III) halides with macrocyclic ethers,[25,28,29] but $[InCl_2(15\text{-crown-5})][InCl_4]$ had only been spectroscopically characterized in anhydrous $SOCl_2$.[27] Thus, in our system the anhydrous hydrogen peroxide merely acted as a high-polarity solvent promoting $InCl_3$ disproportionation. Similar disproportionation was reported for $Et_2O{\cdot}MI_3$ (M = Ga, In) reacting with 18-crown-6.[25] However, $InCl_3$ dissolves sluggishly in diethyl ether despite high ultimate solubility, consistent with the energy required to reorganize the coordination polymer into a molecular monomer.[30] Given the rapid formation of **1**, we hypothesized that 15-crown-5 coordination accelerates $InCl_3$ dissolution in anhydrous H_2O_2. Attempts to replicate this with 18-crown-6, however, yielded an octahedral adduct, $[InCl_3(H_2O_2)(H_2O)_2]{\cdot}$18-crown-6 (**2**) (Fig. 2), rather than the expected ionic product (Scheme 1).

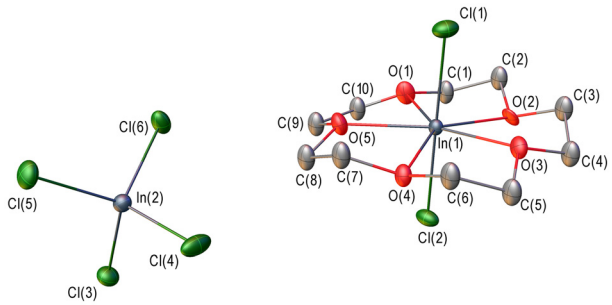

Fig. 1 The asymmetric unit in the crystal structure of **1**. Displacement ellipsoids are shown at 50% probability level. H-atoms of macrocyclic ether and disordered fragment of 15-crown-5 ether are omitted for clarity.

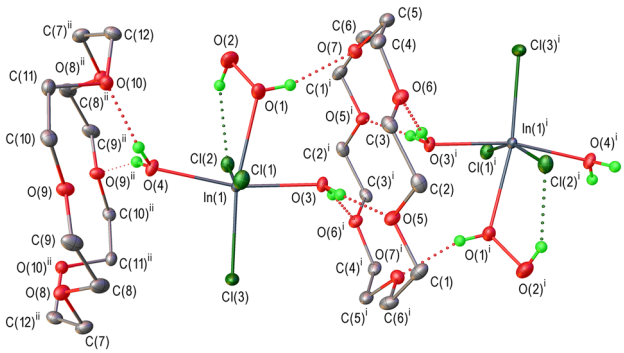

Fig. 2 Fragment of the crystal structure of **2**. Displacement ellipsoids are shown at 50% probability level. H-bonds are shown by dotted line. H-atoms of macrocyclic ether are omitted for clarity. Symmetry operations: (i): $-x+1$; $-y+2$, $-z+1$; (ii): $-x+1$; $-y+1$, $-z$. The asymmetric unit contains one $InCl_3(H_2O_2)(H_2O)_2$ moiety and two crystallographically independent 18-crown-6 molecules lying on an inversion centre.

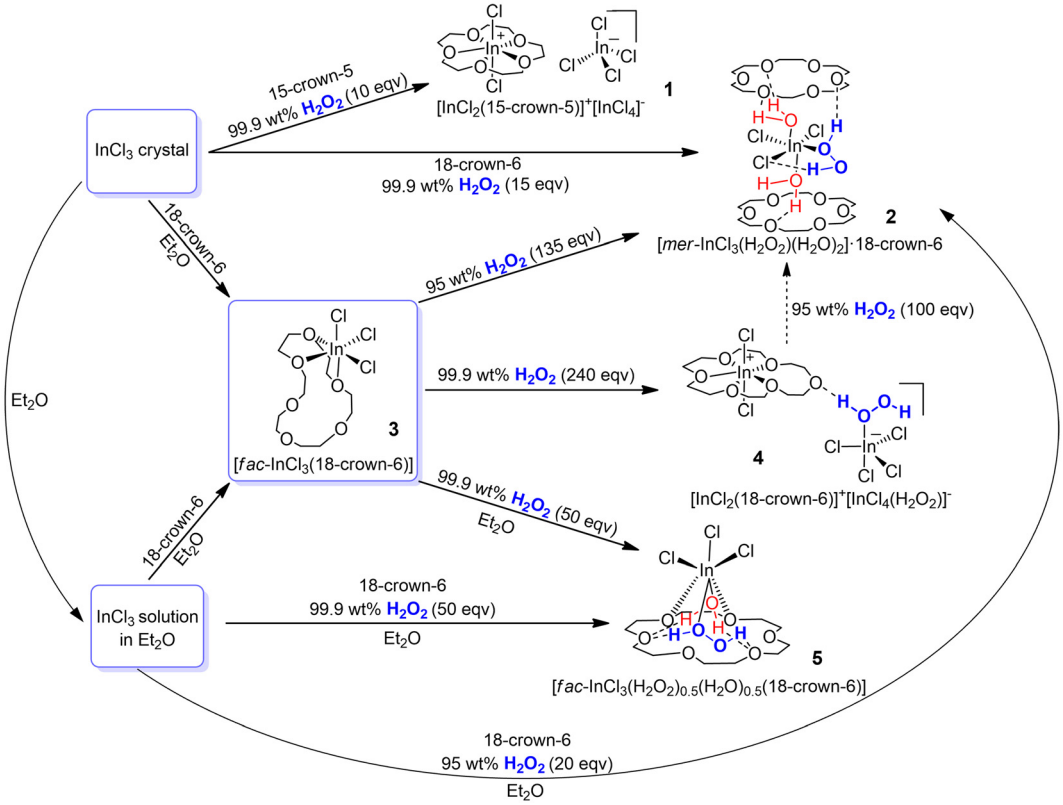

Scheme 1 Complexation of indium trichloride and hydrogen peroxide as confirmed by scXRD.

The indium center in the cation $[InCl_2(15\text{-crown-5})]^+$ adopts a slightly distorted pentagonal bipyramidal geometry (Fig. 1), with In–O distances ranging from 2.216(9) to 2.300(9) Å and In–Cl distances of 2.390(2) and 2.399(2) Å (Table S2). The crown ether is disordered over two positions with a 50/50 occupancy ratio. In contrast to the relatively symmetric cation in **1**, its iodide analogue $[InI_2(18\text{-crown-6})]^+$ exhibits longer In–O distances (2.43–2.96 Å) within a flat oxygen belt.[25] Notably, when 18-crown-6 coordinates to the more acidic $InCl_2^+$, several oxygen atoms become even more loosely bound, potentially forming hydrogen bonds with H_2O_2 (or H_2O produced by peroxide decomposition). This likely facilitates system reorganization, leading to a different complex upon substituting 15-crown-5 with 18-crown-6. In **2**, the coordinated hydrogen peroxide adopts a skew geometry (Fig. 2), with a torsional angle of 108(4)° and an O–O distance of 1.457(2) Å (Table 1 and Table S2), consistent with those in crystalline H_2O_2 [31] and peroxosolvates.[32–34] The In–O_P[P] (O_P[P] – proximal oxygen atom of H_2O_2 coordinated to In) distance (2.469(1) Å) is significantly longer than the In–O_W (O_W – oxygen atom of H_2O coordinated to In) distances (2.215(1) and 2.184(1) Å). For comparison, the In–O_W distances in the crystal structure of the previously described aqua complex [*mer*-$In(H_2O)_3Cl_3$]·18-crown-6 are 2.220(3) and 2.235(4) Å, while in the reported crystal structure of [*fac*-$In(H_2O)_3Cl_3$]·18-crown-6·2H_2O the In–O_W distances are 2.2098(18) Å, 2.219(2) Å and 2.197(2) Å.[35] For the crystalline complex $[In(H_2O)_2Cl_3]$·15-crown-5 In–O_W distances of 2.196 Å and 2.213 Å are reported.[36] Both aqua ligands in **2** form moderately short H-bonds with crown ether oxygens (O_C), with $O_W\cdots O_C$ distances of 2.779(2)–2.841(2) Å (Table S3), typical for non-acidic hydrates. This results in infinite chains of alternating $InCl_3(H_2O_2)(H_2O)_2$ and 18-crown-6 moieties (Fig. 2 and Fig. S3). Coordinated hydrogen peroxide molecule in complex **2** forms two hydrogen bonds: the proximal O–H group is

Table 1 Selected geometric parameters (distances in Å, angles in °) obtained by scXRD analysis characterizing geometry of indium-bound hydrogen peroxide and its hydrogen bonding

				d($O_P\cdots$base)	
Complex	d(In–O_P)	d(O–O)	Torsion angle H–O–O–H	Proximal	Distal
2	2.469(1)	1.457(2)	108(4)	O(1)···O(7) 2.792(2)	O(2)···Cl(2) 3.128(2)
4	2.328(3)	1.464(4)	92(5)	O(7)···O(6) 2.557(4)	O(8)···Cl(6) 3.033(3)
5	2.17(2)	1.470(13)	102(8)	O(1)···O(9) 2.78(2)	O(2)···O(7) 2.602(7)

hydrogen bonded to the crown ether oxygen with an $O_P{}^P\cdots O_C$ distance of 2.792(2) Å, while the distal O–H group interacts with the chloride ligand ($d(O_P{}^d\cdots Cl)$ = 3.128(2) Å, where $O_P{}^d$ – distal oxygen atom of H_2O_2 ligand).

A polycrystalline sample of complex **2** was analyzed by powder X-ray diffraction (pXRD) in perfluorinated oil at room temperature. The resulting pXRD pattern (Fig. S4a) contains reflections that match the crystal structure of complex **2** (marked with asterisks). In addition, the obtained diffractogram contains reflections that presumably correspond to the crystal structure of [*mer*-$InCl_3(H_2O)_3$]·18-crown-6.[35,36] However, the X-ray diffraction pattern recorded from a polycrystalline sample of complex **2** at 100 K on a single-crystal diffractometer is matches the simulated pattern obtained from scXRD data (Fig. S5).

The IR spectrum of complex **2** was virtually identical to that of the previously described triaqua-indium(III) complex [*mer*-$InCl_3(H_2O)_3$]·18-crown-6[35] (Fig. S6), which was additionally synthesized according to the procedure described in the SI and identified by pXRD (Fig. S7). Thus, as with the previously described zinc complex,[20] despite our best efforts, we were unable to detect IR bands that could be attributed to hydrogen peroxide ligands.

The polycrystalline sample of complex **2** was additionally explored by differential thermal analysis (DTA) and thermogravimetry analysis (TGA) (Fig. S8).

The crystallization of $[InCl_3(H_2O)_2(H_2O_2)]$·18-crown-6 (**2**) from an $InCl_3/H_2O_2$/18-crown-6 dispersion might suggest insufficiently dry reagents. However, we used the same batch of 99.9 wt% H_2O_2 to prepare **1** with 15-crown-5. Also, an anhydrous H_2O_2 complex has been isolated previously from a similar $SnCl_4$ system.[22] Thus, water formation likely stems from H_2O_2 decomposition catalyzed by $InCl_3$, consistent with the observed O_2 bubbling. Since $InCl_3$ dissolution in H_2O_2 is apparently initiated by crown ether addition (yielding either anhydrous **1** or aqua-peroxide **2**), we hypothesized that macrocycle coordination accelerates dissolution. However, aqua ligand binding to In(III) may also promote solubility. To accelerate $InCl_3$ dissolution and minimize H_2O_2 decomposition, we decoupled $InCl_3$ monomerization from dissolution in hydrogen peroxide by first synthesizing an anhydrous 18-crown-6 adduct for subsequent H_2O_2 reaction.

Adding an 18-crown-6/Et_2O solution to $InCl_3/Et_2O$ one yielded to formation of complex [*fac*-$InCl_3$(18-crown-6)] (**3**) (Fig. 3). In **3** indium adopts a distorted octahedral geometry, being coordinated by three oxygen atoms of 18-crown-6 (Fig. 3). The In–O_C distances span 2.255(7)–2.321(9) Å, while In–Cl distances are in the range 2.385(3)–2.396 Å (Table S2). Coordination to In(III) severely distorts the macrocycle (Fig. 3). The powder X-ray diffractogram of the obtained polycrystalline sample (Fig. S10) corresponds to the pattern simulated from the scXRD data for complex **3**.

Complex **3** dissolves readily in 99.9 wt% H_2O_2, yielding colorless crystals of the disproportionation product $[InCl_2$(18-crown-6)$]^+[InCl_4(H_2O_2)]^-$ (**4**; Fig. 4) upon storage at −20 °C overnight. The X-ray diffraction pattern recorded from a polycrystalline sample of complex **4** at 100 K on a single-crystal diffractometer is matches the simulated pattern obtained from scXRD data (Fig. S11). Unlike the related 15-crown-5 complex **1**, the $InCl_4^-$ anion in the crystal structure of complex **4** coordinates a hydrogen peroxide molecule (Fig. 4 and Fig. S12). In contrast to its iodide analogue, $[InI_2$(18-crown-6)$]^+$,[25] which features a flat macrocycle, the 18-crown-6 molecule in complex **4** adopts a bent conformation, with one oxygen atom not coordinating the indium(III) center. Instead, this oxygen forms a short hydrogen bond (with the $O_P{}^P\cdots O_C$ separation 2.557(4) Å, Table S3) with the proximal OH group of the H_2O_2 molecule coordinated to the $InCl_4^-$ counterion. This distance is slightly longer than the shortest $O_P{}^P\cdots O_C$ contact in H_2O_2–$SnCl_4$ complexes (2.542(5) Å),[22] indicating enhanced hydrogen bonding

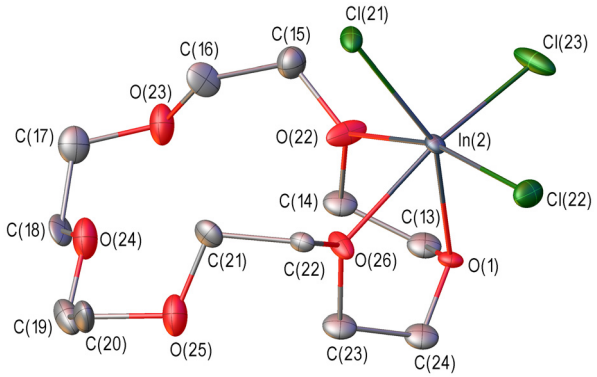

Fig. 3 Fragment of the crystal structures of $InCl_3$ complex with 18-crown-6 ligand (**3**). Displacement ellipsoids are shown at 50% probability level. H-atoms of macrocyclic ether are omitted for clarity. Symmetry operation: (i): $-x + 1$; $-y + 1$, $-z + 1$. The asymmetric unit of **3** is represented by three molecules of [*fac*-($InCl_3$)(18-crown-6)] complex (Fig. S9). The crown ether ligand of one of coordination units is partially disordered between two positions with the 0.626(8)/0.374(8) occupancy ratio.

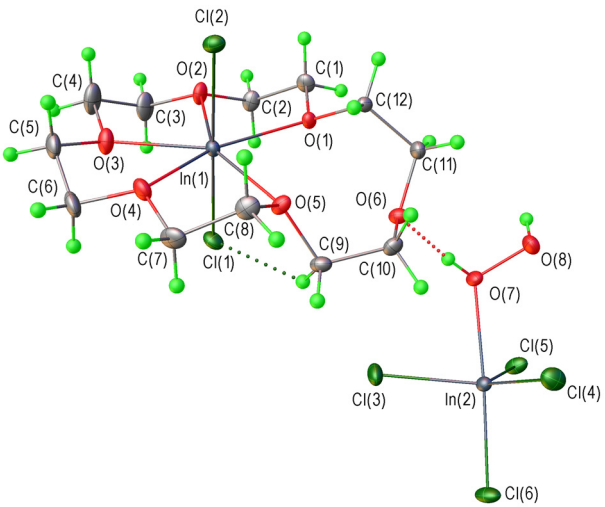

Fig. 4 Asymmetric unit of the crystal structure of **4**. Displacement ellipsoids are shown at 50% probability level.

due to H_2O_2 coordination to the Lewis acid, which stabilizes the peroxide adduct. The distal OH group of the H_2O_2 ligand further engages in a hydrogen bond (3.033(3) Å) with the apical Cl atom of an adjacent $[InCl_4(H_2O_2)]^-$ anion, forming a zig-zag chain (Fig. 5). This $O_P{}^d\cdots Cl$ distance is ~0.1 Å shorter than in complex **2** and in H_2O_2–$SnCl_4$ systems (3.114(4) Å).[22] Concurrently, the $[InCl_2(18\text{-crown-6})]^+$ cations assemble into a separate chain *via* short C–H···Cl interactions between adjacent cations and $[InCl_4(H_2O_2)]^-$ anions (Fig. S12). The disproportionation of indium trichloride in both complexes **1** and **4** appears to be driven by the use of polar hydrogen peroxide as the solvent. The crystal structure of **4** confirms the absence of water, demonstrating that the strategy of employing crystalline adduct **3** as a precursor for the synthesis of an anhydrous indium(III) hydrogen peroxide complex was successful. When water is introduced into the reaction system – for example, by using 95 wt% H_2O_2 instead of anhydrous hydrogen peroxide – the same adduct **3** yields the diaqua hydrogen peroxide complex **2** (Scheme 1). Complex **2** can also be prepared by adding water (10 equivalents per In(III) as 95% hydrogen peroxide) to crystals of complex **4** in the mother liquor (Fig. S13 and Scheme 1). In contrast, adding water (5 equivalents per In (III) as a 0.2 M solution in diethyl ether) to crystals of complex **4** results in the formation of the previously described [*mer*-$InCl_3(H_2O)_3$] 18-crown-6 (Fig. S14).[35]

Crystallization from $InCl_3$–Et_2O–H_2O_2–18-crown-6 ether system

Since the preliminary monomerization of indium(III) chloride as complex **3** proved to be a successful strategy for preparing In(III) hydrogen peroxide complexes from coordinatively saturated crystalline indium(III) chloride, the next step to make was to use a solution of $InCl_3$ in diethyl ether for H_2O_2 complexation, bypassing the crystallization of intermediate **3**. When the solution of 18-crown-6 and 99.9 wt% hydrogen peroxide in ether was added to an ethereal $InCl_3$ solution, the hydrogen peroxide complex [*fac*-$InCl_3(H_2O_2)_{0.5}(H_2O)_{0.5}$]·18-crown-6 (**5**, Fig. 6 and Fig. S15) precipitated. The water content in complex **5** may be attributed to partial decomposition of hydrogen peroxide during the synthesis. The X-ray diffraction pattern obtained from a polycrystalline sample of complex **5** at 100 K on a single crystal diffractometer contains reflections (marked

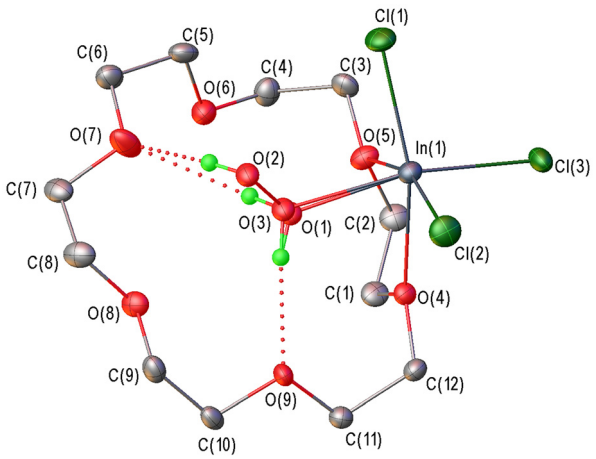

Fig. 6 The asymmetric unit in the crystal structure of **5**. Displacement ellipsoids are shown at 50% probability level. H_2O_2/H_2O occupancy ratio is 50/50. H-atoms of macrocyclic ether are omitted for clarity.

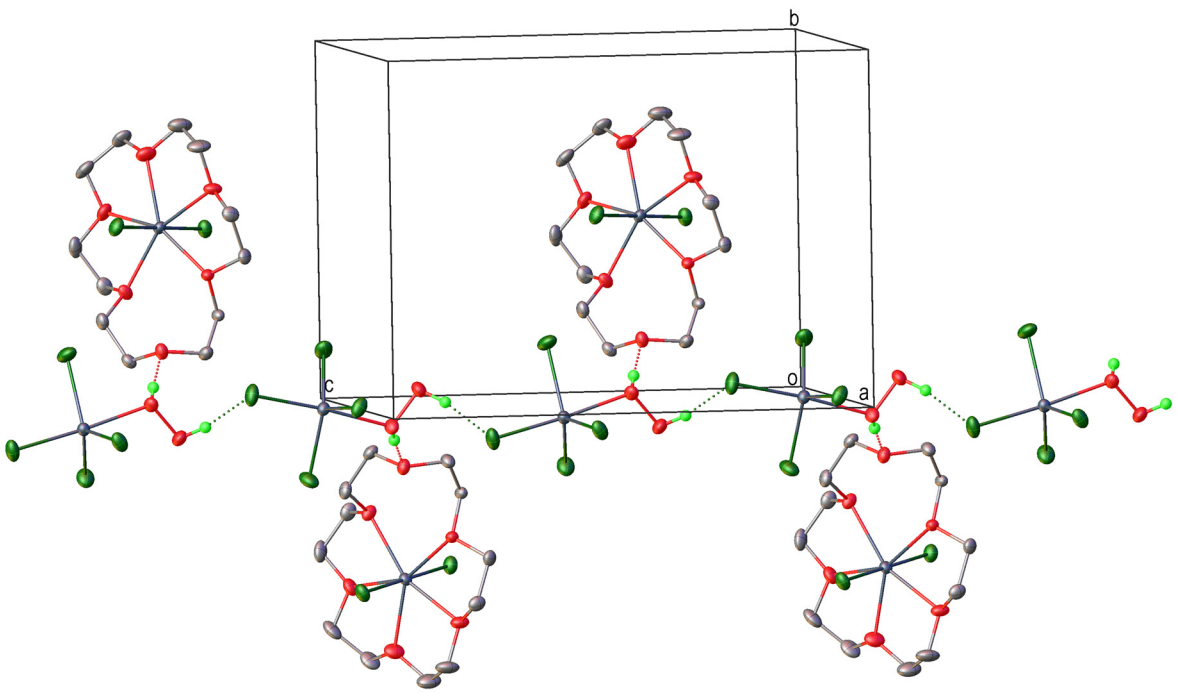

Fig. 5 Supramolecular organization of $[InCl_2(18\text{-crown-6})][InCl_4(H_2O_2)]$ (**4**) in the solid state. H-atoms of macrocyclic ether are omitted for clarity.

with an asterisks) that match the simulated pattern obtained from the scXRD data of complex **5** (Fig. S16).

The scXRD analysis of **5** revealed the H_2O_2/H_2O occupancy ratio of 50/50. The isomorphous substitution of H_2O_2 by H_2O has been well studied in crystalline peroxosolvates[32,34] and was also observed in the zinc–H_2O_2 complex, where the peroxide/water ligand occupancy ratio was 52/48.[20] The In–O_C distances in **5** are 2.283(3) and 2.331(3) Å, similar to those in **3**. The final refinement of the crystal structure of **5** results in the O–O distance in the hydrogen peroxide molecule of 1.470(13), while the In–O_P and In–O_W distances are 2.17(2) and 2.284(19) Å, respectively (Table 1; Table S2). The longer In–O_W distance, as compared to In–O_P, is apparently explained by the O–H···O_C hydrogen bonding of both ligands with the non-disordered crown ether (Fig. 6). In the zinc(II) complex with hydrogen peroxide,[20] the Zn–O_W distance corresponding to the coordination bond of the aqua ligand was also found to be slightly longer compared to that for the hydrogen peroxide ligand, Zn–O_P (2.185(10) and 2.171(10) Å, respectively), despite the disordering of one tosyl group of the second coordination sphere, adapting to the isomorphic substitution of H_2O_2/H_2O.

In **5**, both H_2O and H_2O_2 ligands act as proton donors, forming intramolecular hydrogen bonds with the oxygen atoms of 18-crown-6. As previously established, hydrogen bonds of H_2O_2 possess shorter OH···base distances than those of H_2O in isostructural adducts due to H_2O_2 greater acidity.[34,37] This is also true for the crystal structure of **5**, where the $O_W(H)\cdots O_C$ distances for water are 2.83(2) and 2.97(2) Å, whereas for hydrogen peroxide the donor–acceptor distances $O_P(H)\cdots O_C$ are 2.78(2) Å (proximal OH) and 2.602(7) Å (distal OH) (Table S3). The shorter distal OH hydrogen bond in **5** (*vs.* the proximal one) contrasts with the trends observed in **2**, **4**, and $SnCl_4$–H_2O_2 complexes,[22] likely due to H_2O_2/H_2O isomorphic substitution. This agrees with findings in a zinc(II) complex, where the distal H_2O_2 oxygen formed a shorter hydrogen bond (d(O···O) = 2.552(9) Å) than the proximal one (2.723(15) Å).[20] Thus, the isomorphic substitution of water and hydrogen peroxide ligands results in a discrepancy between their acid–base properties and the geometric parameters of these ligands within the complex – specifically, the distances associated with coordination and hydrogen bonds. This point warrants attention in future analyses of hydrogen peroxide-containing crystal structures.

Interestingly, all attempts to synthesize the hydrogen peroxide complex **4** by altering the reagent ratios in a solution of $InCl_3$ in diethyl ether were unsuccessful – likely due to the low polarity of the reaction system, in which diethyl ether is the predominant solvent. This supports the above hypothesis that the disproportionation of In(III) chloride into $[InCl_2]^+[InCl_4]^-$ is driven by the high polarity of hydrogen peroxide, as observed with other polar solvents (EtOH, CH_3CN, THF) in the presence of auxiliary ligands.[38–40]

In summary, while diethyl ether dissolves crystalline $InCl_3$ (unlike pure anhydrous hydrogen peroxide), the addition of H_2O_2 to the solution causes the ether to lose the competition for In(III) coordination to the weaker ligand, hydrogen peroxide. To investigate this phenomenon we performed ^{1}H NMR experiments and DFT calculations, assuming that hydrogen bonding between H_2O_2 and diethyl ether modifies the properties of H_2O_2. Curiously, nearly a century ago, the formation of an ether–H_2O_2 adduct was proposed based on non-linear density changes and exothermic mixing.[41]

^{1}H NMR spectroscopy

To confirm the formation of ether–H_2O_2 adduct in solution, ^{1}H NMR spectra of 0.03 M solutions of hydrogen peroxide in ether were recorded at different temperatures (Fig. S17). The signal of hydrogen peroxide proton at 25 °C and 0 °C is asymmetric and broadened (Fig. S17a and b), becoming even more complex upon further cooling to −20 °C and −40 °C (Fig. S17c and d). This is probably a result of H_2O_2 self-association and/or its hydrogen bonding with diethyl ether. Cooling the solution shifts the hydrogen peroxide signal downfield from 9.73 ppm at 25 °C to 10.04 ppm at −40 °C (Fig. S17). This is explained by the increased abundance of hydrogen-bonded species, which experience greater deshielding, and a decreased exchange rate.[42,43]

The ^{1}H NMR spectroscopy was used by Wallen and coworkers to study coordination of hydrogen peroxide to a metal center of zinc(II) and cobalt(II) complexes supported by tris(2-tosylamidoethyl)amine (Ts_3tren) ligand.[20,21] It was shown that the addition of 1 equiv. of H_2O_2 solution to a solution of $[n\mathrm{Bu_4N}][(Ts_3\mathrm{tren})Zn^{II}]$ in d_8-THF results in a 0.45 ppm downfield shift of the H_2O_2 proton resonance (9.85 ppm) relative to free H_2O_2 (9.40 ppm) in d_8-THF, which increases with the temperature decrease. These NMR spectral data indicate the H_2O_2 coordination and strong intramolecular hydrogen bonding in its complex with zinc.[20] Similar experiments for $[n\mathrm{Bu_4N}][(Ts_3\mathrm{tren})Co^{II}]$ complex revealed the appearance of a broad signal at 5.9 ppm, which shifted downfield to 8.8 ppm (closer to that of free H_2O_2 at 9.4 ppm) over time due to the decomposition of H_2O_2. The authors concluded that this shifted H_2O_2 resonance is the first direct evidence that H_2O_2 is binding to Co^{II}.[21]

To find out whether H_2O_2 forms complex with $InCl_3$ in diethyl ether we performed ^{1}H NMR studies in analogous manner by adding 1 equiv. H_2O_2 to $InCl_3$ solution (0.03 M) at 0 °C. ^{1}H NMR spectrum of this solution revealed 0.1 ppm downfield shift of H_2O_2 proton resonance compared to free H_2O_2 in diethyl ether (Fig. 7; see Fig. S18 for full spectra). This can be attributed to the coordination of the hydrogen peroxide molecule to indium(III), which alters the effective deshielding of H_2O_2 protons. Moreover, the addition of indium trichloride to the system induces more than tenfold broadening of the H_2O_2 signal, with the line shape becoming symmetric (Fig. 7). At −40 °C, the full width at half-maximum (FWHM) increases from 3.9 Hz for H_2O_2 alone to 41.9 Hz in presence of the $InCl_3$ (molar ratio 1 : 1); at 0 °C, it rises from 1.6 to 12.7 Hz. This is consistent with chemical exchange of hydrogen peroxide protons that became non-equivalent due to the κ^1-coordination of H_2O_2 with In(III). The enhancement of the proton

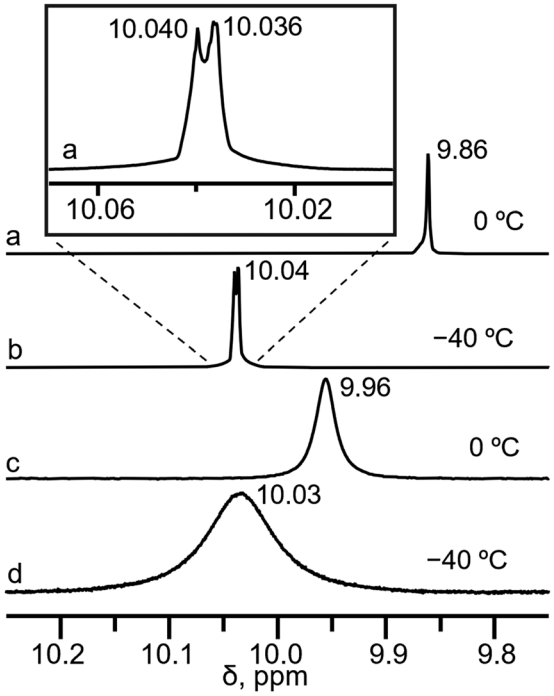

Fig. 7 Fragments of ^{1}H NMR spectra of H_2O_2 in Et_2O (0.03 M) at 0 °C (a), −40 °C (b) and its equimolar mixture with $InCl_3$ in Et_2O at 0 °C (c) and −40 °C (d).

exchange process can be caused by an increase in the acidity of H_2O_2 due to coordination with indium(III).

Our attempts to apply the ^{115}In NMR method to characterize the complexation of indium chloride were unsuccessful due to the high quadrupole moment of the ^{115}In nucleus. Details are presented in the SI—in Fig. S19 and in characterization section.

DFT calculations

DFT calculations at the ω-B97xD/Def2-TZVPP theory were performed using dimethyl ether (Me_2O) and diethyl ether (Et_2O) as model ethers (see SI for more details). All the computed complexation energies (ΔE), enthalpies (ΔH) and Gibbs free energies (ΔG) are gathered in Table S4. Herein we mainly discuss the complexes formation enthalpies, which are less sensitive to the entropic contribution, together with the σ-lumps (*i.e.*, molecular electrostatic potential (MEP) minima), serving as a measure of atomic basicity.[44] For instance, the MEP minima for ether oxygen in Me_2O and Et_2O are −35.5 and −36.6 kcal mol^{-1}, respectively, while those for H_2O and H_2O_2 are of comparable magnitude but differ by several units (Table 2). Hydrogen peroxide exhibits lower basicity than water, with MEP minima of −33.4 and −39.5 kcal mol^{-1}, respectively, making H_2O the preferred base for binding acidic sites. Conversely, both water and hydrogen peroxide can act as proton donors in hydrogen bonds, with H_2O_2 dominating such interactions due to its more acidic protons. This is consistent with the identical dimerization enthalpies (ΔH° = −2.8 kcal mol^{-1}) for H_2O and H_2O_2 dimers featuring a single O–H···O bond,

Table 2 MEP minima values (V_S, min, in kcal mol^{-1}) on oxygen atoms of water, hydrogen peroxide and their hydrogen bonded complexes. Complex formation enthalpies (ΔH, in kcal mol^{-1})[a]

	V_S, min	ΔH
H_2O	−39.5	
$(H_2O)_2$	−48.5	−2.8
H_2O_2	−33.4	
Linear $(H_2O_2)_2$	−43.4	−2.8
Cyclic $(H_2O_2)_2$	−29.0	−4.5
H–O–H···O_2H_2	−48.9	−1.8
HO–O–H···OH_2	−44.6	−4.2
H_2O·im[b]	−59.5	−5.1
H_2O_2·im[b]	−54.5	−7.5
Et_2O	−36.6	
Me_2O	−35.5	
HO–O–H···OEt_2	−45.6	−5.7
HO–O–H···OMe_2	−45.8	−4.9
O_2H_2···2(OMe_2)	−56.1	−10.5
H–O–H···OMe_2	−50.6	−3.5
OH_2···2(OMe_2)	−58.7	−7.4

[a] Calculated at the ωB97XD/def2-TZVPP level relative to the isolated reactants in water. [b] im = imidazole.

whereas the hydrogen bond from water to peroxide, O–H_W···O_P, is less favorable than the reverse O–H_P···O_W (Table 2).[45,46]

Hydrogen bonding through an OH group proton increases the basicity of the participating oxygen. For example, the σ-lump on H_2O_2 oxygen becomes 21.1 kcal mol^{-1} more negative upon hydrogen bonding with imidazole (a model base used to study H_2O_2 coordination to Sn(IV)[22]) surpassing the basicity of free H_2O by as much as 15 kcal mol^{-1}. In the H_2O_2–H_2O complex where hydrogen peroxide is a proton donor, O–H_P···O_W, the enhanced peroxide oxygen's σ-lump (−44.6 kcal mol^{-1}) exceeds that of both free H_2O and linear H_2O_2 dimer (−43.4 kcal mol^{-1}; Fig. 8, left). Thus, trace water in neat H_2O_2 should enhance its basicity and ability to coordinate the Lewis acids. A similar effect occurs with ethers, though their intrinsic basicity is only 2–3 kcal mol^{-1} higher than free H_2O_2 (but lower than H_2O). Coordination to one Me_2O molecule raises the H_2O_2 oxygen σ-lump to −45.8 kcal mol^{-1} (Table 2), while a second Me_2O nearly doubles this effect (−56.1 kcal mol^{-1}; Fig. 8, right). Consequently, H_2O_2 activated by O–H_P···O hydrogen bonds with ethers becomes a superior Lewis base compared to isolated H_2O_2 or its dimer. We leveraged this phenomenon when synthesizing $InCl_3$–H_2O_2 complexes from diethyl ether solutions (*vide supra*). However, ether solutions must exclude water, as ether activates H_2O in a similar manner as H_2O_2, rendering H_2O an even stronger base (Table 2).

We probed also hydrogen peroxide's ability to form complexes with $[InCl_4]^-$, which serves as an excellent model for studying base coordination. This anion features a single primary coordination site (the quadruply degenerate σ-hole of the tetrahedral structure), whose occupation stabilizes a trigonal bipyramidal geometry. As an anionic Lewis acid (formally an electrophile), $[InCl_4]^-$ exhibits high sensitivity to base strength. Although the electrostatic potential at the 0.001 a.u. van der Waals surface of this compact anion is uniformly nega-

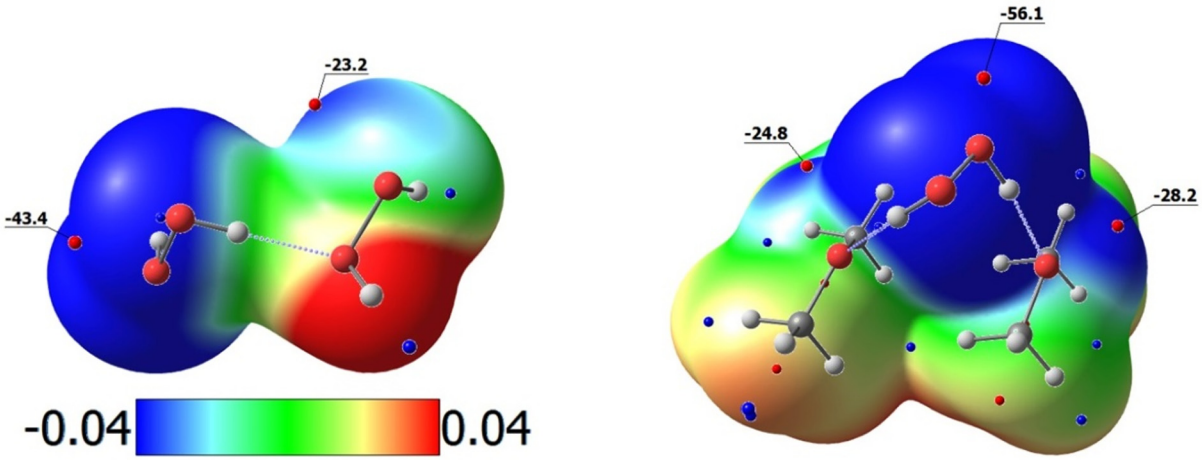

Fig. 8 The molecular electrostatic potential (MEP) surface at 0.001 a.u. for linear H_2O_2 dimer (left) and hydrogen bonded complex of H_2O_2 with two Me_2O molecules (right). MEP minima ($V_{S,\ min}$, in kcal mol^{-1}) are shown as red dots, blue dots correspond to the MEP maxima.

tive due to its overall charge, we still could identify a local MEP maximum ($V_{S,\ max}$) positioned along the In–Cl bond axis on the tetrahedron's opposite face coinciding with the σ^*_{InCl} orbital location (Fig. S20). Despite its negative $V_{S,\ max}$ value, these σ-holes serve as binding sites for bases, as illustrated by complexes with H_2O_2 (Fig. 9). A single H_2O_2 molecule forms an exceptionally weak complex (ΔH = −0.6 kcal mol^{-1}) that barely perturbs $[InCl_4]^-$ tetrahedral geometry (Fig. 9).

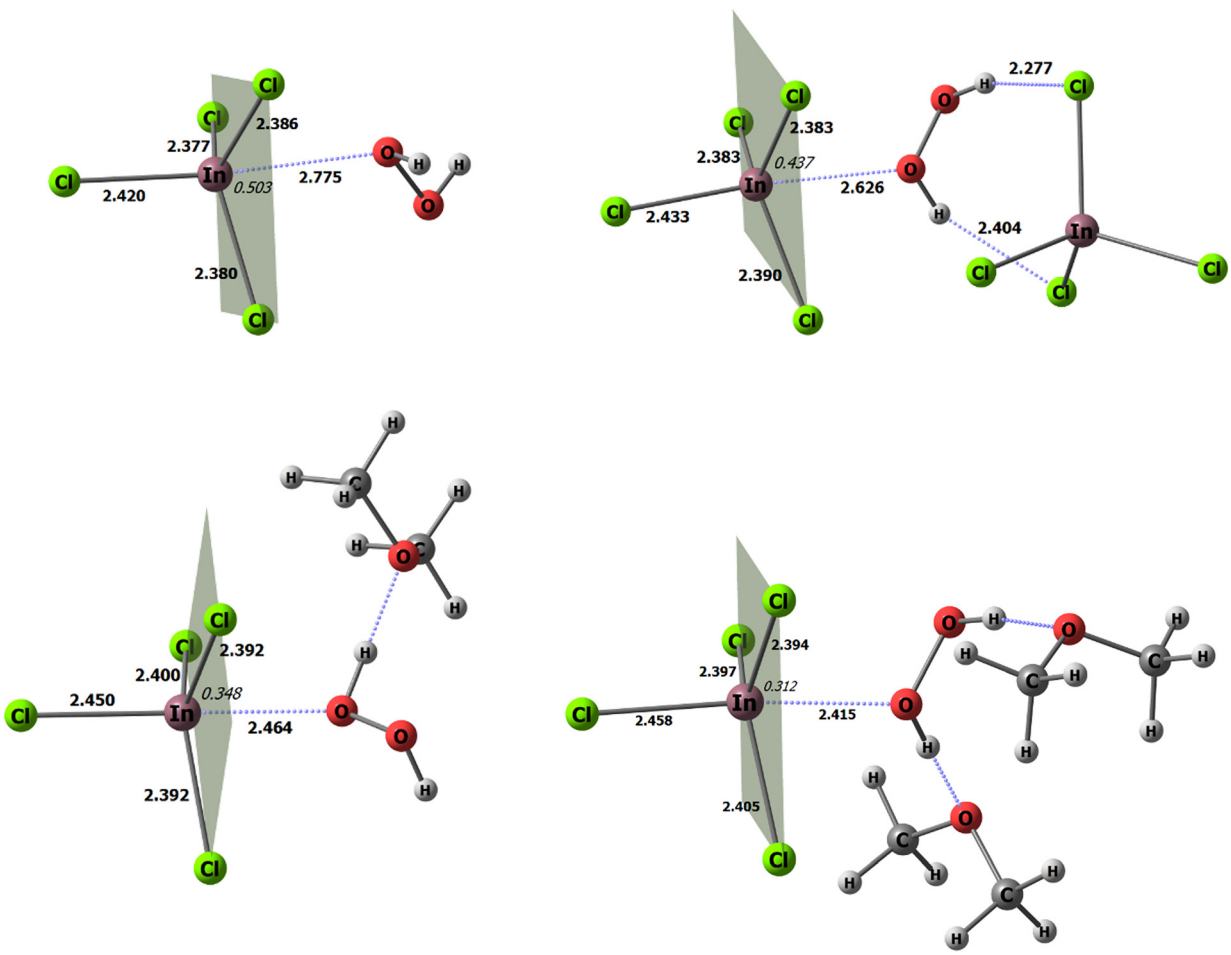

Fig. 9 Structures of $[InCl_4]^-$ Lewis adducts with H_2O_2 with principal distances (Å). Deviations of In atom from Cl_3 plane are in italic.

Intriguingly, "self-activation" *via* hydrogen bonding to a second $[InCl_4]^-$ anion only marginally strengthens the complex (ΔH = −1.8 kcal mol^{-1}). This limited enhancement reflects indium tetrachloride poor hydrogen-bond affinity for H_2O_2 (ΔH = −4.1 kcal mol^{-1} for two O–H_P···Cl bonds), yielding negligible basicity amplification. In contrast, H_2O_2 activated by H-bonding to one or two Me_2O molecules forms significantly more stable complexes (ΔH = −4.0 and −4.8 kcal mol^{-1}, respectively, relative to solvated species), featuring shorter In–O_P distances and a pronounced shift toward a bipyramidal geometry (Fig. 9 and Fig. S21).

Conclusions

This work demonstrates that the synthetic approach using neat hydrogen peroxide and crown ethers for preparing and crystallizing H_2O_2 complexes of compounds soluble in hydrogen peroxide can be extended to reactions with coordinatively saturated compounds, such as solid indium(III) chloride. The diaqua hydrogen peroxide complex $[InCl_3(H_2O)_2(H_2O_2)]$·18-crown-6 (**2**) was crystallized from a dispersion of solid $InCl_3$ in H_2O_2 after adding 18-crown-6. Since crystalline $InCl_3$ is insoluble in H_2O_2, we propose that 18-crown-6 coordination facilitates its dissolution. Indeed, the pre-synthesized $InCl_3$–18-crown-6 adduct (**3**) readily dissolves in H_2O_2 and reassembles, yielding the complex $[InCl_2(18\text{-crown-6})][(H_2O_2)InCl_4]$ (**4**), where H_2O_2 coordinates to the anionic Lewis acid $[InCl_4]^-$. Anhydrous H_2O_2 acts as a high-polarity solvent, promoting $InCl_3$ disproportionation into $[InCl_2]^+[InCl_4]^-$. This is corroborated by the crystallization of $[InCl_2(15\text{-crown-5})][InCl_4]$ (**1**) from neat H_2O_2. The absence of H_2O_2 ligands in **1** stems from the reduced basicity of all 15-crown-5 oxygens upon In(III) coordination, whereas in **4**, one uncoordinated 18-crown-6 oxygen forms a hydrogen bond with H_2O_2. This interaction activates H_2O_2, enhancing its oxygen's coordination to $[InCl_4]^-$ as supported by DFT calculations.

Diethyl ether (Et_2O) emerged as a unique solvent for dissolving coordinatively saturated precursors and synthesizing H_2O_2 complexes. Although Et_2O typically outcompetes H_2O_2 in coordination to Lewis acids, their mixture reverses this trend due to O–H_P···O hydrogen bonding, which amplifies H_2O_2 basicity. A similar mechanism likely applies to crown ethers. This principle enabled the crystallization of $[fac\text{-}InCl_3(H_2O_2)_{0.5}(H_2O)_{0.5}(18\text{-crown-6})]$ (**5**) from Et_2O. Notably, complex **2** was also prepared by reacting $InCl_3/Et_2O$ with 95 wt% aqueous H_2O_2, eliminating the need for pure H_2O_2 as a solvent. This Et_2O-based route significantly improves the accessibility and safety of H_2O_2 complexes synthesis.

Author contributions

Nikita S. Mayorov: investigation, methodology, formal analysis, writing – original draft. Pavel A. Egorov: investigation, methodology, formal analysis, writing – original draft. Alexander G. Medvedev: project administration, investigation, methodology, formal analysis, writing – original draft. Evgeny S. Belyaev: investigation (NMR); Oleg A. Filippov: conceptualization, investigation (DFT), methodology, software, formal analysis writing – original draft, writing – review & editing. Natalia V. Belkova: conceptualization, investigation (IR), methodology, formal analysis writing – original draft, writing – review & editing. Alexey A. Mikhaylov: investigation, methodology, formal analysis writing – original draft, Maxim N. Sokolov: writing – review & editing, Ovadia Lev: conceptualization, writing – review & editing and Petr V. Prikhodchenko: project administration, conceptualization, supervision, writing – review & editing.

Conflicts of interest

There are no conflicts to declare.

Data availability

The data supporting this article have been included as part of the supplementary information (SI). Supplementary information is available. See DOI: https://doi.org/10.1039/d6dt00780e.

CCDC 2381797 (**1**), 2355318 (**2**), 2431051 (**3**), 2431052 (**4**) and 2431053 (**5**) contain the supplementary crystallographic data for this paper.[47a–e]

Acknowledgements

This work was supported by the Russian Science Foundation (grant no. 22-13-00426-П). IR spectra were measured on the equipment of the Center for Collective Use of INEOS RAS operating under support of the Ministry of Science and Higher Education of the Russian Federation (Contract No. 075-03-2026-024). The X-ray diffraction studies were performed using the equipment of the JRC PMR IGIC RAS. The NMR studies were performed using the equipment of the CKP FMI IPCE RAS.

References

1 M. D. Brand, Mitochondrial generation of superoxide and hydrogen peroxide as the source of mitochondrial redox signaling, *Free Radicals Biol. Med.*, 2016, **100**, 14–31.
2 D. L. Nelson and M. M. Cox, *Lehninger Principles of Biochemistry*, W.H. Freeman and Company, New York, 8th edn, 2021.
3 K. Sengupta, S. Chatterjee and A. Dey, Catalytic H_2O_2 disproportionation and electrocatalytic O_2 reduction by a functional mimic of heme catalase: direct observation of compound 0 and compound I in situ, *ACS Catal.*, 2016, **6**(3), 1382–1388.
4 S. Bhunia, A. Rana, S. G. Dey, A. Ivancich and A. Dey, A designed second-sphere hydrogen-bond interaction that

critically influences the O–O bond activation for heterolytic cleavage in ferric iron–porphyrin complexes, *Chem. Sci.*, 2020, **11**, 2681–2695.

5 J. Jia, B. Wang, A. Wu, G. Cheng, Z. Li and S. Dong, A method to construct a third-generation horseradish peroxidase biosensor: self-assembling gold nanoparticles to three-dimensional sol-gel network, *Anal. Chem.*, 2002, **74**(9), 2217–2223.

6 V. P. Pandey, M. Awasthi, S. Singh, S. Tiwari and U. N. Dwivedi, A comprehensive review on function and application of plant peroxidases, *Biochem. Anal. Biochem.*, 2017, **6**, 1000308.

7 S. Wu, R. Snajdrova, J. C. Moore, K. Baldenius and U. T. Bornscheuer, Biocatalysis: enzymatic synthesis for industrial applications, *Angew. Chem., Int. Ed.*, 2021, **60**(1), 88–119.

8 B. O. Burek, S. Bormann, F. Hollmann, J. Z. Bloh and D. Holtmann, Hydrogen peroxide driven biocatalysis, *Green Chem.*, 2019, **21**, 3232–3249.

9 G. R. Lopes, D. C. G. A. Pinto and A. M. S. Silva, Horseradish peroxidase (HRP) as a tool in green chemistry, *RSC Adv.*, 2014, **4**, 37244–37265.

10 J. Karam and J. A. Nicell, Potential applications of enzymes in waste treatment, *J. Chem. Technol. Biotechnol.*, 1996, **69**(2), 141–153.

11 A. A. Karyakin, Catalytic properties of peroxidase mimicking nanozymes, *Russ. Chem. Rev.*, 2023, **92**(8), RCR5088.

12 Y. Huang, J. Ren and X. Qu, Nanozymes: classification, catalytic mechanisms, activity regulation, and applications, *Chem. Rev.*, 2019, **119**(6), 4357–4412.

13 L. Gao, K. Fan and X. Yan, Iron oxide nanozyme: a multifunctional enzyme mimetic for biomedical applications, *Theranostics*, 2017, **7**(13), 3207–3227.

14 M. L. Kuznetsov, Y. N. Kozlov, D. Mandelli, A. J. L. Pombeiro and G. B. Shul'pin, Mechanism of Al^{3+}-catalyzed oxidations of hydrocarbons: dramatic activation of H_2O_2 toward O-O homolysis in complex $[Al(H_2O)_4(OOH)(H_2O_2)]^{2+}$ explains the formation of $HO^{\bullet}$ radicals, *Inorg. Chem.*, 2011, **50**(9), 3996–4005.

15 A. S. Novikov, M. L. Kuznetsov, A. J. L. Pombeiro, N. A. Bokach and G. B. Shul'pin, Generation of $HO^{\bullet}$ radical from hydrogen peroxide catalyzed by aqua complexes of the group III metals $[M(H_2O)_n]^{3+}$ (M = Ga, In, Sc, Y, or La): a theoretical study, *ACS Catal.*, 2013, **3**(6), 1195–1208.

16 S. A. Mirza, B. Bocquet, C. Robyr, S. Thomi and A. F. Williams, Reactivity of the coordinated hydroperoxo ligand, *Inorg. Chem.*, 1996, **35**(5), 1332–1337.

17 M. G. Evans and N. Uri, The dissociation constant of hydrogen peroxide and the electron affinity of the HO_2 radical, *Trans. Faraday Soc.*, 1949, **45**, 224.

18 A. G. DiPasquale and J. M. Mayer, Hydrogen peroxide: a poor ligand to gallium tetraphenylporphyrin, *J. Am. Chem. Soc.*, 2008, **130**(6), 1812–1813.

19 G. A. Kirakosyan, S. V. Loginov, T. V. Galuzina, V. Tarasov and Y. A. Buslaev, An NMR study of the solvation of ions in anhydrous peroxide, *Russ. J. Inorg. Chem.*, 1990, **35**(9), 1314.

20 C. M. Wallen, J. Bacsa and C. C. Scarborough, Hydrogen peroxide complex of zinc, *J. Am. Chem. Soc.*, 2015, **137**(46), 14606–14609.

21 C. M. Wallen, L. Palatinus, J. Bacsa and C. C. Scarborough, Hydrogen peroxide coordination to cobalt(II) facilitated by second-sphere hydrogen bonding, *Angew. Chem.*, 2016, **128**(39), 12081–12085.

22 A. G. Medvedev, P. A. Egorov, A. A. Mikhaylov, E. S. Belyaev, G. A. Kirakosyan, Y. G. Gorbunova, O. A. Filippov, N. V. Belkova, E. S. Shubina, M. N. Brekhovskikh, A. A. Kirsanova, M. V. Babak, O. Lev and P. V. Prikhodchenko, Synergism of primary and secondary interactions in a crystalline hydrogen peroxide complex with tin, *Nat. Commun.*, 2024, **15**, 5758.

23 D. T. Richens, *The Chemistry of Aqua Ions: Synthesis, Structure and Reactivity: A Tour through the Periodic Table of the Elements*, Wiley, 1997.

24 D. H. Templeton and G. F. Carter, The crystal structures of yttrium trichloride and similar compounds, *J. Phys. Chem.*, 1954, **58**(11), 940–944.

25 L. A. Kloo and M. J. Taylor, Complexes of a crown ether with gallium(III) iodide and indium(III) iodide, *J. Chem. Soc., Dalton Trans.*, 1997, 2693–2696.

26 M. J. Taylor, D. G. Tuck and L. Victoriano, Co-ordination compounds of indium. Part 38. Complexes of indium(I) and indium(III) with macrocyclic ligands, *J. Chem. Soc., Dalton Trans.*, 1981, 928–932.

27 L. Kloo and M. J. Taylor, Spectroscopic characterisation of indium(III) chloride and mixed ligand complexes, *Spectrochim. Acta, Part A*, 2002, **58**(5), 953–957.

28 J. L. Atwood, S. G. Bott and M. T. May, Synthesis and crystal structure of $[(ClAl(\mu\text{-}OH)_2AlCl)\cdot 18\text{-Crown-6}][AlCl_4]_2\cdot 8/3\,C_6H_5NO_2$, a complex featuring a binuclear aluminum-containing cation threaded through 18-crown-6, *J. Coord. Chem.*, 1991, **23**(1–4), 313–320.

29 M. L. Cole, R. Haigh and C. Jones, The molecular structure of $[TlCl_2(18\text{-Crown-6})][TlCl_4]$, *Main Group Met. Chem.*, 2001, **24**, 819–820.

30 F. Fairbrother, N. Flitcroft and H. Prophet, Complex compounds of indium trihalides Part I. Ether complexes, *J. Less-Common Met.*, 1960, **2**(1), 49–63.

31 J. M. Savariault and M. S. Lehmann, Experimental determination of the deformation electron density in hydrogen peroxide by combination of X-ray and neutron diffraction measurements, *J. Am. Chem. Soc.*, 1980, **102**(4), 1298–1303.

32 A. G. Medvedev, A. V. Churakov, P. V. Prikhodchenko, O. Lev and M. V. Vener, Crystalline peroxosolvates: nature of the coformer, hydrogen-bonded networks and clusters, intermolecular interactions, *Molecules*, 2021, **26**(1), 26.

33 D. A. Grishanov, M. A. Navasardyan, A. G. Medvedev, O. Lev, P. V. Prikhodchenko and A. V. Churakov, Hydrogen peroxide insular dodecameric and pentameric clusters in peroxosolvate structures, *Angew. Chem., Int. Ed.*, 2017, **56**(48), 15241–15245.

34 I. Yu. Chernyshov, M. V. Vener, P. V. Prikhodchenko, A. G. Medvedev, O. Lev and A. V. Churakov, Peroxosolvates:

formation criteria, H_2O_2 hydrogen bonding, and isomorphism with the corresponding hydrates, *Cryst. Growth Des.*, 2017, **17**(1), 214–220.

35 A. B. Ilykhin, Z. V. Dobrokhotova and S. P. Petrosyants, Isomerization of $[In(H_2O)_3Cl_3]$ 18C6. Crystal Structure of $[mer\text{-}In(H_2O)_3Cl_3]\cdot 18C6$ and $[fac\text{-}In(H_2O)_3Cl_3]\cdot 18C6\cdot 2H_2O$, *Russ. J. Coord. Chem.*, 2008, **34**, 641–646.

36 N. R. Strel'tsova, M. G. Ivanov, S. D. Vashchenko, V. K. Bel'skij and I. I. Kalinichenko, Synthesis of indium(3) chloride complexes with crown ethers and crystal structure of $InCl_3\cdot 2H_2O\cdot 15C5$ and $InCl_3\cdot 3H_2O\cdot 18C6$, *Koord. Khim.*, 1991, **17**(5), 646.

37 M. V. Vener, A. G. Medvedev, A. V. Churakov, P. V. Prikhodchenko, T. A. Tripol'skaya and O. Lev, H-bond network in amino acid cocrystals with H_2O or H_2O_2. The DFT study of serine-H_2O and serine-H_2O_2, *J. Phys. Chem. A*, 2011, **115**(46), 13657–13663.

38 W. T. Robinson, C. J. Wilkins and Z. Zeying, Structures of indium trihalide complexes with phosphine oxides and dimethyl sulphoxide, with comments on the metal-oxygen bonding, *J. Chem. Soc., Dalton Trans.*, 1990, 219–227.

39 X. Du, R. Fan, X. Wang, L. Qiang, P. Wang, S. Gao, H. Zhang, Y. Yang and Y. Wang, Combined effect of hydrogen bonding and π···π stacking interactions in the assembly of indium(III) metal-organic materials: structure-directing and aggregation-induced emission behavior, *Cryst. Growth Des.*, 2015, **15**(5), 2402–2412.

40 J. Takaya and N. Iwasawa, Synthesis, structure, and catalysis of palladium complexes bearing a Group 13 metalloligand: remarkable effect of an aluminum-metalloligand in hydrosilylation of CO_2, *J. Am. Chem. Soc.*, 2017, **139**(17), 6074–6077.

41 E. P. Linton and O. Maass, The dielectric constants of hydrogen peroxide-ether and hydrogen peroxide-water mixtures, *Can. J. Res.*, 1931, **4**(4), 322–329.

42 P. J. Berkeley Jr. and M. W. Hanna, Nuclear Magnetic Resonance Studies of Hydrogen Bonding. II. Calculation of the Shift upon Complex Formation, *J. Am. Chem. Soc.*, 1964, **86**(15), 2990–2994.

43 G. A. Jeffrey, *An Introduction to Hydrogen Bonding*, Oxford University Press, New York, 1997, pp. 303.

44 S. Scheiner, D. L. Cooper, M. Kohout and M. L. Kuznetsov, Comparison of bifurcated halogen with hydrogen bonds, *Molecules*, 2021, **26**(2), 350.

45 Energies of O_W–H_W, O_W–H_P, O_P–H_W and O_P–H_P complexes nicely fit to the results of MD simulations of water/peroxide mixtures in ref. 46.

46 C. Parida and S. Chowdhuri, Effects of hydrogen peroxide on the hydrogen bonding structure and dynamics of water and its influence on the aqueous solvation of the insulin monomer, *J. Phys. Chem. B*, 2023, **127**(50), 10814–10823.

47 (*a*) CCDC 2381797: Experimental Crystal Structure Determination, 2026, DOI: 10.5517/ccdc.csd.cc2kyg55; (*b*) CCDC 2355318: Experimental Crystal Structure Determination, 2026, DOI: 10.5517/ccdc.csd.cc2k1x0k; (*c*) CCDC 2431051: Experimental Crystal Structure Determination, 2026, DOI: 10.5517/ccdc.csd.cc2mlq0z; (*d*) CCDC 2431052: Experimental Crystal Structure Determination, 2026, DOI: 10.5517/ccdc.csd.cc2mlq10; (*e*) CCDC 2431053: Experimental Crystal Structure Determination, 2026, DOI: 10.5517/ccdc.csd.cc2mlq21.